Geochemistry Geophysics Geosystems G3
AN ELECTRONIC JOURNAL OF THE EARTH SCIENCES
Published by AGU and the Geochemical Society

Data Brief
Volume 4, Number 6
27 June 2003
8910, doi:10.1029/2002GC000435
ISSN: 1525-2027

Composition of altered oceanic crust at ODP Sites 801 and 1149

Katherine A. Kelley and Terry Plank
Department of Earth Sciences, Boston University, 685 Commonwealth Ave., Boston, Massachusetts 02215, USA (kelleyk@bu.edu; tplank@bu.edu)

John Ludden
INSU/SDU - CNRS, 3, rue Michel-Ange BP 287, 75766 Paris Cedex 16, France (john.ludden@cnrs-dir.fr)

Hubert Staudigel
Institute of Geophysics and Planetary Physics, Scripps Institution of Oceanography, University of California, San Diego, La Jolla, California 92093, USA (hstaudigel@ucsd.edu)

[1] We present a comprehensive major and trace element dataset establishing ODP Site 801 as a geochemical reference for altered oceanic crust. The composition of old crustal sequences like those at Sites 801 and 1149 are critical to developing models of crustal aging and seawater chemistry evolution and to understanding the fate of crust consumed at subduction zones. Our estimate of the bulk composition of oceanic crust at Site 801 comprises ICP-AES and ICP-MS analyses of 117 discrete samples, 14 mixed composites and 5 glasses from the upper 500 m of Jurassic Pacific crust. Comparing the 801 "super-composite" with glass reveals enrichment of U (5x), Li (2x), K_2O (4x), Rb (9x), and Cs (7x), similar to DSDP Sites 417/418, but little to no enrichment in Ba or Pb. The data also demonstrate good (~10%) agreement between U measured on discrete samples and natural gamma logs, suggesting logging data is a reliable means of establishing bulk geochemical characteristics of oceanic crust. Data reported here serve to link other geochemical and mineralogical measurements on Site 801 and 1149 samples. We also document Boston University sample preparation procedures and instrument parameters for ICP-MS and ICP-AES analyses, and provide comparisons with other laboratories and techniques. We present new techniques for basaltic glass analyses using the Boston University 213 nm Nd-YAG LA-ICP-MS system, and show the data agree well with both solution-ICP-MS (5–10%) and ion probe measurements (~10%).

Components: 5472 words, 6 figures, 9 tables, 2 data sets.

Keywords: Alteration; MORB; ICP-AES; ICP-MS; LA-ICP-MS; subduction.

Index Terms: 1020 Geochemistry: Composition of the crust; 1030 Geochemistry: Geochemical cycles (0330); 1065 Geochemistry: Trace elements (3670).

Received 1 September 2002; **Revised** 21 February 2003; **Accepted** 21 February 2003; **Published** 27 June 2003.

Kelley, K. A., T. Plank, J. Ludden, and H. Staudigel, Composition of altered oceanic crust at ODP Sites 801 and 1149, *Geochem. Geophys. Geosyst.*, *4*(6), 8910, doi:10.1029/2002GC000435, 2003.

Theme: Oceanic Inputs to the Subduction Factory **Guest Editors:** Terry Plank and John Ludden

1. Introduction

[2] The composition of old oceanic crust bears on many problems in earth sciences, ranging from the deep biosphere to the deep mantle. Altered oceanic crust (AOC) is of particular interest to geochemistry because it moderates ocean chemistry and contributes mass and chemical components to subduction zone fluids and the deeper mantle. AOC may be a significant CO_2 sink, holding consequences for atmospheric and oceanic CO_2 levels and the global carbon cycle [*Staudigel et al.*, 1989; *Alt and Teagle*, 1999]. Subducted AOC also contributes a geochemical signature to arc volcanics and the continental crust [*Ishikawa and Nakamura*, 1994; *Miller et al.*, 1994], while the residual slab may create mantle heterogeneity [*Hofmann and White*, 1982; *Chauvel and Hémond*, 2000].

[3] While the importance of AOC to the evolution of Earth's crust and mantle has long been recognized, little work has focused on determining bulk geochemical characteristics of aged oceanic crust. Existing bulk alteration studies have focused on three drill sites: DSDP/ODP Sites 417/418, 504B, and 735B. Site 504B, located in 7 Ma Costa Rica Rift crust, is the only site to penetrate the upper 2 km of in-situ oceanic crust [*Alt et al.*, 1996]. The young age of 504B, however, makes it less suitable for subduction discussions since the mean age of subducting crust is significantly older (~60 Ma) [*Jarrard*, 1986]. Site 735B extends 1.5 km into 11–12 Ma oceanic gabbros exposed along a fracture zone on the SWIR and provides the primary reference for gabbroic alteration [*Bach et al.*, 2001]. Sites 417/418 are located in 118 Ma [*Cande and Kent*, 1995], slow-spreading Atlantic crust and, until now, the 417/418 "super composite" constituted the only estimate widely used for bulk AOC geochemical budgets [*Hart and Staudigel*, 1989; *Staudigel et al.*, 1989, 1995, 1996].

[4] A primary goal of ODP Leg 185 was to sample old, Pacific AOC to complement Sites 504B and 417/418. Leg 185 deepened pre-existing Hole 801C and initiated Site 1149 (Figure 1). Together, the two sites embody end-member characteristics of AOC (old, fast spreading) and provide valuable references for crustal input to the Izu-Bonin-Mariana subduction zone. Site 801 lies in 170 Ma, fast spreading crust (15 cm/yr [*Bartolini and Larson*, 2001]) east of the Mariana Islands, in the subducting Pacific plate, and drilling during Leg 129 recovered the first Jurassic MORB in the Pacific [*Lancelot et al.*, 1990]. Leg 185 deepened 801C to a total of 470 m into basement [*Plank et al.*, 2000] with high average recovery (50%). The igneous sequence at Site 801 is capped by 60 m of younger, alkalic basalt (157 Ma) separated from normal MORB pillows and flows by a 20 m silicic hydrothermal deposit. Site 1149 sits east of the Izu-Bonin arc, northeast of and along the same spreading compartment as Site 801. Hole 1149D penetrates 133 m into Cretaceous (135 Ma) basement and contains thin, fractured and brecciated units contributing to low average recovery (20%). Leg 129 sample analyses [*Castillo et al.*, 1992] and Leg 185 shipboard XRF analyses [*Plank et al.*, 2000] were performed on minimally-altered samples to establish primary igneous characteristics of the sites, whereas we collected samples aiming to capture bulk characteristics of AOC. Remarkably, both Leg 185 sites recovered pristine MORB glass [*Fisk and Kelley*, 2002], providing the necessary baseline to assess alteration.

2. Samples

[5] Characterizing the composition of AOC is difficult, due partially to heterogeneous distribution and incomplete recovery of altered materials within the crust, but also to individual core sampling by scientists with differing objectives. For example, one study may address isotopic variations in certain samples while another utilizes different samples for trace element studies, producing datasets that are difficult to relate. The Leg 185 science party developed an integrated sampling plan that involved taking a set of shared "common" samples representing major lithologies (massive flows, pillows, interflow material and breccia) and alteration styles (veins, haloes, minimally and pervasively altered basalt, glass) while satisfying numerous scientific objectives.

[6] Common samples can be used in two ways to determine large-scale chemical budgets in

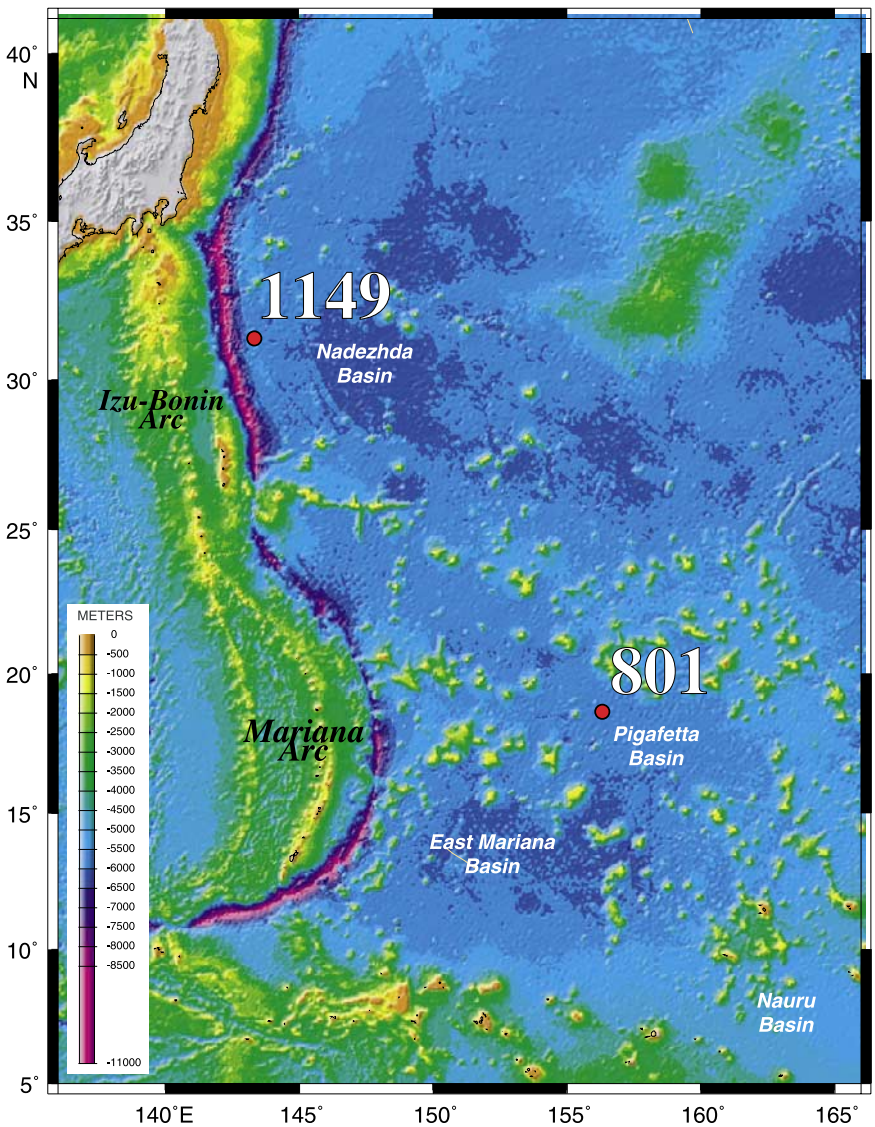

Figure 1. Map of the western Pacific showing locations of ODP Sites 801 and 1149 [from *Plank et al.*, 2000].

Table 1a. Solution and LA-ICP-MS Settings

Element	Mass	Detector Mode
Li	7	Pulse Count
Be	9	Pulse Count
Sc	45	Analog
Ti	47, 49	Analog
V	51	Analog
Cr	52	Analog
Co	59	Analog
Ni	60	Analog
Cu	65	Analog
Zn	66	Analog
Ga	69	Analog
Rb	85	Pulse Count
Sr	86	Analog
Zr	89	Analog
Y	90	Analog
Nb	93	Pulse Count
Cs	133	Pulse Count
Ba	135, 137	Pulse Count
La	139	Pulse Count
Ce	140	Pulse Count
Pr	141	Pulse Count
Nd	146	Pulse Count
Sm	147	Pulse Count
Eu	151	Pulse Count
Gd	160	Pulse Count
Tb	159	Pulse Count
Dy	163	Pulse Count
Ho	165	Pulse Count
Er	166	Pulse Count
Yb	172	Pulse Count
Lu	175	Pulse Count
Hf	178	Pulse Count
Ta	181	Pulse Count
Pb	208	Pulse Count
Th	232	Pulse Count
U	238	Pulse Count

Instrument Settings (VG Plasma Quad ExCell)	Solution	Laser
	Gas Flows, L/min	
Cool Gas	12.5–13.0	12.5–13.0
Auxiliary	0.80–1.00	0.80–1.00
Nebulizer	0.82–0.90	1.00–1.50
	Lens Settings, Volts	
Extraction	−1000	−1000
Collector/D1	−33.0–39.2	−41.4
L1	+1.6–7.6	+1.0
L2	−114.4–169.0	−119.3
L3	−94.1–115.8	−94.1
L4/Focus	+15.8–22.0	+12.4
Pole Bias	+3.0	−3.5
	Vacuums, mbar	
Expansion	1.4–1.7	1.4–1.7
Analyzer	$<9.0 \times 10^{-7}$	$<9.0 \times 10^{-7}$
RF Power, W	1350	1200
Pts/Pk	3	1
DAC Step	5	5

Table 1a. (continued)

Dwell Time, μsec	10.24	10.24
Analysis Settings	Solution	Laser
Sample Uptake Time	120 s	0 s
Acquisition Time	60 × 3 s	180 s
Rinse Time	120 s	0 s
Acquisition Mode	Peak jump	Peak jump
Average Sensitivity	100,000 cps/ppb (^{115}In)	2500 cps/ppm (^{139}La)
Average Oxides	2.5% (^{156}CeO/^{140}Ce)	7.0% (^{248}ThO/^{232}Th)
Average Ba^{++}/Ba	5.5% ($^{69}Ba^{++}/^{138}$Ba)	
Low Mass Background (5)	<1	<1
High Mass Background (220)	<1	<1
Laser Settings		
Repeat Rate (Hz)	10	
Beam Energy (mJ/pulse)	0.65	
Spot Size (μm)	125	
Beam Expander (%)	0	
Iris (%)	20	

AOC. Individual sample data may be mixed mathematically by calculating a weighted average of the composition of AOC. Alternatively, powders may be mixed physically, according to their proportions in the core, generating large-volume composites that may be analyzed themselves [*Staudigel et al.*, 1996]. These approaches have different practical and scientific benefits. Physical composites require fewer analyses to achieve meaningful results, and large sample volumes permit the application and correlation of many analytical techniques. Once the composites are mixed, however, individual sample contributions cannot be resolved. Analyzing discrete samples reveals how elements vary on small scales within the crust and illuminates processes controlling the bulk composition. Our approach is between these extremes. Simpler measurements like major and trace elements were first performed on individual common samples to guide both in constructing composite mixtures and in interpreting their final compositions. Several composite samples were prepared to capture larger-scale crustal heterogeneity between different depth intervals and

between less-altered and highly-altered lithologies. In constructing the recipes for the composite mixtures (see data table A in auxiliary material), we used visual estimates from the recovered cores, downhole natural gamma and formation microscanner (FMS) logs, and the geochemical data for the common samples to determine the relative contribution of each sample to the composites.

[7] Thirty samples from Site 1149 and 117 samples from Site 801 make up the common sample set and composite source material. Three types of samples characterize the altered basalt at these sites: minimally altered, average and highly altered. We selected minimally-altered samples from each major igneous unit. Fifty samples from Site 801 represent average altered portions of the core in terms of color, halo structure, and vein type. We also sampled highly altered inter-flow material based on lithology (sedimentary or igneous), color, and texture. Samples were taken as 3–6 cm quarter-core sections, split into three slabs for powdering, thin sectioning, and archiving. We recorded size, color and proportions of primary and secondary minerals in each slab slated for powdering. On the JOIDES *Resolution*, we removed surface contamination on all samples by sandblasting with alumina grit, eroding 0.1–0.5 mm from all surfaces. Sandblasted slabs were sonicated for 10–20 min in de-ionized water and air dried. Site 801 samples were crushed between two Delrin discs in a hydraulic press by applying 5–8 tons of pressure. Chips were freeze-dried for 3 hours, then powdered for 15 min in an alumina ball-mill. Site 1149 samples were powdered at CRPG, Nancy, France, using an agate shatterbox without prior crushing. The composites were also mixed at CRPG by weighing individual sample powders according to the recipe (see data table A in auxiliary material) and homogenizing them in an agate shatterbox.

3. Analytical Methods

[8] Sample preparation and analytical procedures for solution-based analyses of all samples follow techniques developed for analyzing basalt and sediment [*Plank and Ludden*, 1992; *Elliott et al.*, 1997; *Balzer*, 1999; *Johnson and Plank*, 1999] (www.bu.edu/es/Research/index.html). Sample dissolution for inductively coupled plasma mass spectrometry (ICP-MS) analysis involves HF-HNO_3 acid digestion carried out in class 100 hoods, using acids distilled in-house [*Mattinson*, 1972]. First, the analyst weighs 0.05 g of powder into 23 mL Savillex Teflon beakers, then adds 3 mL of 8N HNO_3 and 1 mL of HF to each beaker. Samples are digested overnight at 90°C on a hot plate and then evaporated to dryness. Dried samples are re-dissolved in 3 mL of 8N HNO_3 and 3 mL of de-ionized (>18.2 MΩ) water, transferred to HDPE bottles and diluted by weight with de-ionized water to 2000× the original powder weight, then sonicated for 30 min. Omitting HCl and $HClO_4$ from the digestion minimizes interferences (e.g. $^{40}Ar^{1}H^{35}Cl^{16}O_4$ on ^{140}Ce), and

Table 1b. ICP-AES Settings

Instrument Settings (Jobin Yvon Ultrace 130C)	L/min			
	Gas Flows			
P1 (Cool)	12–13			
G1 (Sheath)	0.2–0.3			
G2 (Alkali sheath)	0.6			
Nebulizer	0.5–1.0			
RF Power	1000 W			
Element	Wavelength (nm)	Bkg (nm)	Voltage	Gain
P	178.229		830	3
Ni	231.604	+0.032	840	3
Si	251.611		680	2
Mn	257.610		700	3
Fe	259.940		690	2
Cr	267.716	−0.048	900	3
Mg	285.213		570	3
Cu	324.754	−0.0459, +0.0339	930	3
Ti	334.941		630	3
Zr	343.823	−0.0479	900	3
Y	371.030	−0.046	860	3
Ca	393.366		610	1
Al	396.152		660	3
Sr	407.771		700	3
Ba	455.403		830	3
Na	589.592		860	3
K	766.490		990	3
Analysis Settings	Sec			
Sample Uptake Time	90			
Acquisition Time	140 × 3			
Rinse Time	90			

Table 2. Comparison of KU and BU Solution ICP-MS Data

	801C-23R-3-80-84			801C-31R-4-43-45			801C-43R-1-13-15		
Lab (cm)	BU	KU	Difference, %	BU	KU	Difference, %	BU	KU	Difference, %
Li	10.0	9.55	−4.7%	7.60	7.39	−2.8%	10.3	9.70	−6.0%
Be	0.561	0.512	−8.9%	0.730	0.691	−5.3%	0.695	0.635	−8.5%
Sc	48.9	48.8	−0.2%	45.8	44.5	−2.8%	46.7	45.6	−2.3%
TiO2 (%)	2.24	2.20	−1.8%	2.26	2.24	−1.1%	2.04	1.97	−3.7%
V	437	455	4.2%	428	425	−0.6%	411	421	2.4%
Cr	107	102	−5.0%	104	104	−0.3%	85.2	80.0	−6.0%
Co	42.0	41.2	−2.0%	44.0	43.4	−1.3%	48.0	45.8	−4.8%
Ni	46.8	46.5	−0.5%	49.0	48.9	−0.1%	48.1	46.9	−2.6%
Cu	72.1	68.5	−5.1%	65.3	67.6	3.6%	67.5	63.3	−6.2%
Zn	117	112	−3.9%	117	117	0.1%	108	105	−2.6%
Ga	19.3	19.5	1.1%	18.1	18.4	1.4%	18.6	18.8	1.4%
Rb	0.213	0.194	−9.0%	0.284	0.275	−3.5%	0.432	0.434	0.3%
Sr	128	122	−4.6%	108	106	−1.8%	118	114	−3.4%
Y	46.7	45.2	−3.3%	54.0	53.7	−0.4%	44.6	43.2	−3.0%
Zr	150.9	146	−3.0%	157	157	0.0%	135	131	−3.3%
Nb	4.43	4.28	−3.5%	3.91	3.91	0.0%	3.54	3.46	−2.2%
Ba	9.96	9.95	−0.1%	12.4	12.2	−1.4%	11.8	11.8	−0.7%
La	4.43	4.38	−1.1%	4.53	4.65	2.6%	3.88	3.92	1.1%
Ce	14.7	14.5	−1.2%	15.1	15.5	2.8%	13.1	13.1	0.0%
Pr	2.62	2.60	−0.8%	2.69	2.83	5.5%	2.33	2.38	1.8%
Nd	14.2	14.0	−1.5%	15.0	15.3	2.1%	13.0	12.9	−1.2%
Sm	4.92	4.85	−1.5%	5.28	5.41	2.4%	4.59	4.51	−1.6%
Eu	1.70	1.70	0.2%	1.77	1.81	2.4%	1.58	1.58	−0.2%
Gd	6.73	6.77	0.6%	7.31	7.57	3.5%	6.30	6.38	1.2%
Tb	1.23	1.22	−1.4%	1.35	1.40	3.7%	1.16	1.16	−0.5%
Dy	7.82	7.72	−1.3%	8.65	8.92	3.1%	7.43	7.42	−0.1%
Ho	1.71	1.69	−0.8%	1.93	1.94	0.4%	1.65	1.64	0.0%
Er	4.77	4.72	−0.9%	5.43	5.53	1.8%	4.63	4.66	0.6%
Yb	4.56	4.46	−2.2%	5.38	5.50	2.2%	4.71	4.66	−1.0%
Lu	0.705	0.691	−2.0%	0.841	0.851	1.2%	0.739	0.733	−0.7%
Hf	4.13	4.15	0.4%	4.31	4.30	−0.1%	3.75	3.83	2.0%
Ta	0.308	0.308	0.2%	0.292	0.284	−2.7%	0.259	0.261	0.6%
Pb	0.388	0.394	1.7%	2.36	2.49	5.1%	0.771	0.803	4.1%
Th	0.245	0.254	3.7%	0.216	0.223	3.5%	0.196	0.207	5.8%
U	0.108	0.110	1.8%	0.0865	0.0867	0.3%	0.0830	0.0847	2.1%
Average			2.4%			2.1%			2.4%

Comparison of geochemical measurements of unknown samples by ICP-MS at Boston University (BU) and the University of Kansas (KU). Analyses were performed on solutions made from separate aliquots of powder treated with the same acid digestion procedures (see text). Elements in ppm. Average Difference, % calculated using absolute values of reported differences. External precision averages 2–2.5% based on these data.

Table 3. Standard Values Used for Calibration

	Primary Standards					Secondary Standards								Standard Run as Unknown			
Name	AGV-1	BHVO-1	BIR-1	DNC-1	W-2	JA-1	JR-1	K1919	MAR	BIR-1G	BHVO-2G	BCR-2G		JB-3	Average	% 2σ	% diff.
Rock Type	Andesite	Basalt	Basalt	Diabase	Diabase	Andesite	Rhyolite	Basalt	Basalt	Basaltic glass	Basaltic glass	Basaltic glass	Chondrite	Basalt Accepted	(n = 6) ICP-AES		
SiO_2	60.02	49.94	47.77	47.04	52.44	64.06	76.40	50.00	49.59					50.96	51.24	0.7%	0.5%
TiO_2	1.07	2.67	0.96	0.48	1.06	0.87	0.101	2.70	1.226	0.869	2.60	2.25		1.44	1.36	1.6%	−5.8%
Al_2O_3	17.49	13.8	15.35	18.3	15.35	14.98	13.06	13.85	15.24					17.20	17.27	0.6%	0.4%
Fe_2O_3	6.91	12.23	11.26	9.93	10.74	6.95	0.973	12.28	11.11					11.82	11.72	1.5%	−0.9%
MnO	0.0918	0.17	0.171	0.149	0.163	0.15	0.0912	0.17	0.18					0.177	0.178	1.0%	0.8%
MgO	1.56	7.26	9.68	10.05	6.37	1.61	0.0912	7.01	9.09					5.19	5.15	1.3%	−0.7%
CaO	5.04	11.26	13.24	11.27	10.87	5.68	0.638	11.36	11.36					9.79	9.81	0.4%	0.2%
Na_2O	4.35	2.26	1.75	1.87	2.14	3.86	4.15	2.36	2.56					2.73	2.80	0.4%	2.5%
K_2O	2.98	0.52	0.027	0.229	0.627	0.78	4.47	0.54	0.09					0.780	0.788	0.4%	1.0%
P_2O_5	0.500	0.273	0.046	0.085	0.131	0.16	0.0203	0.28	0.114					0.294	0.297	1.4%	0.9%
															ICP-MS		
Li	11.3	4.9	3.4	5.1	9.7	10.5	61.4	4.95	5.629	3.16	4.60	9.91		7.21	7.95	1.0%	10.2%
Be	2.38	1.1	0.114	0.225	0.74	0.564	50.3	1.1	0.403	0.100	1.22	2.84		0.810	0.778	3.1%	−3.9%
Sc	12.2	31.6	42.35	31	35	28.4	5.16	30.3	39.3	40.2	30.8	34.3		33.8	33.3	2.2%	−1.5%
V	121	317	313	157	262	105	7	304	261	294	299	407		372	370	1.5%	−0.6%
Cr	10.1	289.5	382	285	93	7.3	2.3	245	321	371	288	13.8		58.1	57.5	4.4%	−1.0%
Co	15.3	45	51.4	56	44	11.8	0.65	49.3	53.4	47.7	43.0	38.7		34.3	35.2	2.7%	2.6%
Ni	16	120	166	256	70	1.8	0.66	98	150.9	151	112	11.5		36.2	36.0	2.9%	−0.5%
Cu	60	150	122.5	96	111	42.2	1.4	145	73.7	109	131	28.2		194	196	2.2%	1.0%
Zn	88	100	71	66	77	90.6	30	98	78.4	13.5	20.6	34.7		100	103	1.8%	2.6%
Ga	20	21	15.25	13.7	17.3	17.3	17.6	21	15	59.2	96.1	149		19.8	20.5	4.6%	3.4%
Rb	68	9.2	0.23	3.9	22	12	257	10.352	0.933	0.187	9.76	51.9		15.1	16.0	1.6%	6.0%
Sr	668	399	107.5	144.5	197	266	30	398	91.9	104	388	347		403	407	1.8%	1.0%
Y	20	27.1	15.5	17.7	21.9	30.6	45.4	26.9	31.7	14.8	26.2	38.0		26.9	26.7	1.4%	−0.7%
Zr	244	184	15.2	36.9	93.1	88.3	101	186	79.1	14.8	180	206		97.8	100	1.6%	2.7%
Nb	14.9	19.7	0.546	1.47	7.7	1.32	15.5	20.054	1.43	0.543	19.2	13.6		2.47	2.18	2.7%	−11.8%

Table 3. (continued)

	Primary Standards					Secondary Standards								Standard Run as Unknown			
Name	AGV-1	BHVO-1	BIR-1	DNC-1	W-2	JA-1	JR-1	K1919	MAR	BIR-1G	BHVO-2G	BCR-2G		JB-3	Average	% 2σ	% diff.
Cs	1.26	0.0967	0.004	0.207	0.902	0.658	20.2	0.095	0.0264	0.00483	0.0965	1.18		0.940	0.960	0.5%	2.1%
Ba	1226	132.86	6.63	103.3	171.62	307	40	135	6.55	6.14	129	674		245	241	0.9%	−1.7%
La	38.7	15.74	0.56	3.56	10.07	4.88	19.7	15.056	2.027	0.544	15.0	25.7	0.329	8.81	7.86	3.1%	−10.8%
Ce	69	37.77	1.9	8.11	22.79	13.2	47.1	38.528	6.98	1.75	36.8	54.0	0.855	21.5	21.0	2.8%	−2.2%
Pr	8.5	5.4	0.39	1.12	3.04	2.21	5.62	5.583	1.34	0.362	5.29	7.02	0.130	3.11	3.37	1.6%	8.4%
Nd	32.3	24.81	2.4	4.98	12.9	11	23.5	25.115	7.37	2.23	24.2	29.7	0.630	15.6	15.7	1.9%	1.0%
Sm	5.82	6.1	1.11	1.43	3.24	3.44	6.07	6.195	2.79	1.01	5.92	6.75	0.203	4.27	4.23	1.4%	−0.8%
Eu	1.73	1.98	0.52	0.57	1.1	1.17	0.3	2.074	1.023	0.459	1.94	2.07	0.0770	1.32	1.32	1.3%	−0.1%
Gd	4.9	6.56	1.98	2.11	3.73	4.4	5.24	6.408	4.14	1.76	6.32	7.36	0.276	4.67	4.71	1.0%	0.8%
Tb	0.706	0.948	0.381	0.399	0.632	0.780	0.948	1.004	0.757	0.321	0.950	1.13	0.0511	0.730	0.773	0.8%	5.9%
Dy	3.78	5.37	2.62	2.76	3.83	4.9	5.78	5.483	5.11	2.28	5.34	6.79	0.343	4.54	4.69	1.5%	3.3%
Ho	0.698	1.01	0.59	0.62	0.8	1.07	1.1	1.018	1.13	0.526	0.984	1.38	0.0770	0.800	0.965	2.0%	20.6%
Er	1.87	2.38	1.71	1.87	2.17	3.03	3.78	2.568	3.24	1.48	2.46	3.75	0.225	2.49	2.68	1.5%	7.6%
Yb	1.7	2.01	1.7	1.97	1.98	3.02	4.49	2.065	3.18	1.51	2.02	3.60	0.220	2.55	2.55	2.1%	−0.1%
Lu	0.262	0.29	0.26	0.32	0.3	0.475	0.71	0.298	0.494	0.236	0.296	0.562	0.0339	0.390	0.394	1.5%	0.9%
Hf	5.17	4.49	0.596	0.995	2.48	2.69	4.67	4.772	2.17	0.564	4.45	5.27		2.67	2.88	1.0%	7.8%
Ta	0.9	1.21	0.045	0.095	0.5	0.111	1.9	1.4	0.234	0.0455	1.19	0.864		0.150	0.153	3.0%	2.2%
Pb	37	2.055	2.88	6.2	7.7	5.74	19.1	1.096	0.312	2.98	1.66	10.9		5.58	5.13	1.7%	−8.1%
Th	6.5	1.247	0.031	0.24	2.1	0.758	26.5	1.234	0.093	0.0280	1.19	6.23		1.27	1.28	2.8%	1.1%
U	1.92	0.4083	0.0085	0.05	0.49	0.345	9	0.42	0.067	0.0749	0.412	1.70		0.480	0.474	2.5%	−1.3%

Oxides in weight percent, all other elements in ppm. Primary standard values based on assessment of data reported in *Cheatham et al.* [1993], *Jochum et al.* [1994], *Jenner et al.* [1990], *Eggins et al.* [1997], *Elliott et al.* [1997] and White (unpublished ID-TIMS). Nb and Ta determined by Plank, using the method of standard additions-ICP-MS and NBS standards 3155 (Ta) and 3137 (Nb). Zr and Hf determined by isotope dilution-ICPMS by Plank. Secondary standard values based on calibration to primary standards. Chondrite values are modified from *Nakamura* [1974], and are used for normalizing REE (Figure 4). JB-3 accepted values are from *Imai et al.* [1996].

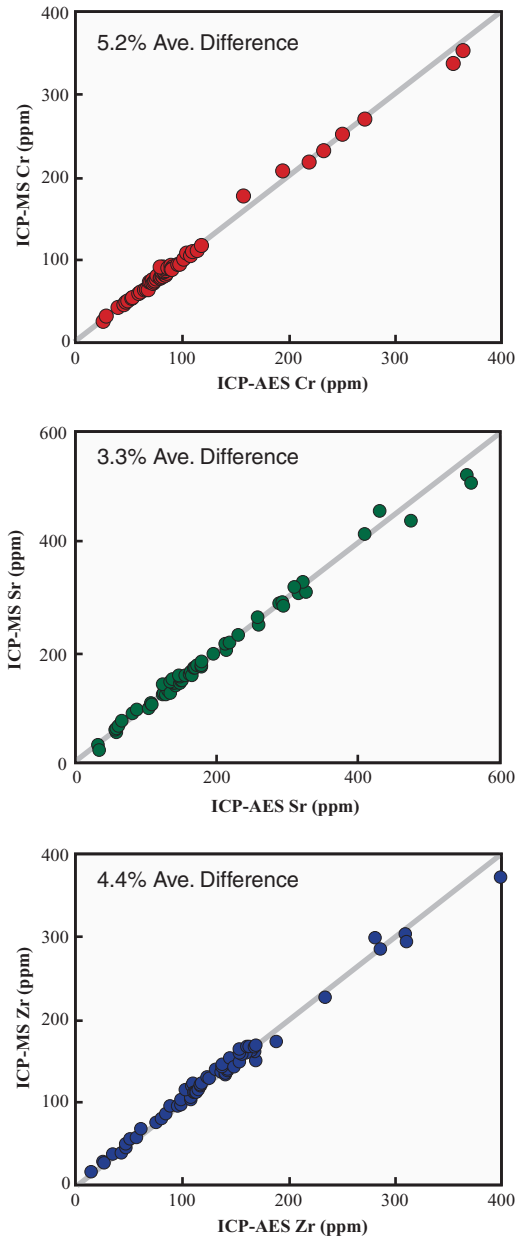

Figure 2. Comparison of Cr, Sr and Zr concentrations measured using ICP-MS and ICP-AES at Boston University. Gray lines are 1:1 correlation, and average difference between the data sets is $\leq$5%. The two data sets are based on analyses of aliquots of the same sample powders prepared using completely different methods (acid digestion for ICP-MS, flux-fusion for ICP-AES; see text). ICP-MS data are corrected for LOI because flux fusions were performed on ignited powders whereas acid digestions were not. This comparison provides a quantitative check on both the different preparation and instrumental techniques.

keeping evaporation temperatures low retains some HF, which holds Nb and Ta in solution. This procedure is thus advantageous because there are few steps (taking ~3 days), few molecular interferences, and solutions are stable for up to a year.

[9] Digestion for inductively coupled plasma atomic emission spectrometry (ICP-AES) analysis requires a different procedure, due to Si-loss as volatile SiF_4 from HF-HNO_3 digests. ICP-AES solutions are prepared using $LiBO_2$ flux-fusions [*Klein et al.*, 1991; *Miller et al.*, 1992]. Powders are first dried by weighing 0.2 g of each sample into alumina crucibles, placing them in a 100°C muffle furnace for 1 hour, then recording the dry weight. After drying, the crucibles are placed in a muffle furnace at 950°C for 45 min, then weighed to measure the mass loss on ignition (LOI). The analyst weighs 0.1 g of ignited powder into high-purity graphite crucibles containing 0.4 g of $LiBO_2$ flux, mixes the sample and flux together, and places the crucibles into a 1050°C muffle furnace for 15 min. Molten beads are poured into HDPE bottles containing 50 mL of 5% HNO_3, then shaken until fully dissolved. These solutions are drawn into syringes and 10 mL of solution are expelled through 0.45 μm filters into HDPE bottles containing 70 mL of 5% HNO_3, generating solutions diluted ~4300× the original sample weight and ~860× the weight of total solids.

[10] Trace elements were measured using either the Boston University VG PQ ExCell quadrupole ICP-MS or the University of Kansas VG PQIIXS quadrupole ICP-MS. All samples were run using identical sample preparation and data reduction protocols, operating conditions and instrument settings (Table 1a). Data from the two facilities agree within <5% for most elements (Table 2). ICP-MS data are acquired using one of two detector settings. The pulse count setting amplifies ion signals through a series of discrete dynodes, each dynode creating an electron "pulse" when hit by an ion or electron, and is used for measuring low-abundance elements (<5 ppb in solution). The analog setting intercepts the electron pulse from a dynode halfway along the detector, and is used on higher-abundance elements (>5 ppb in solu-

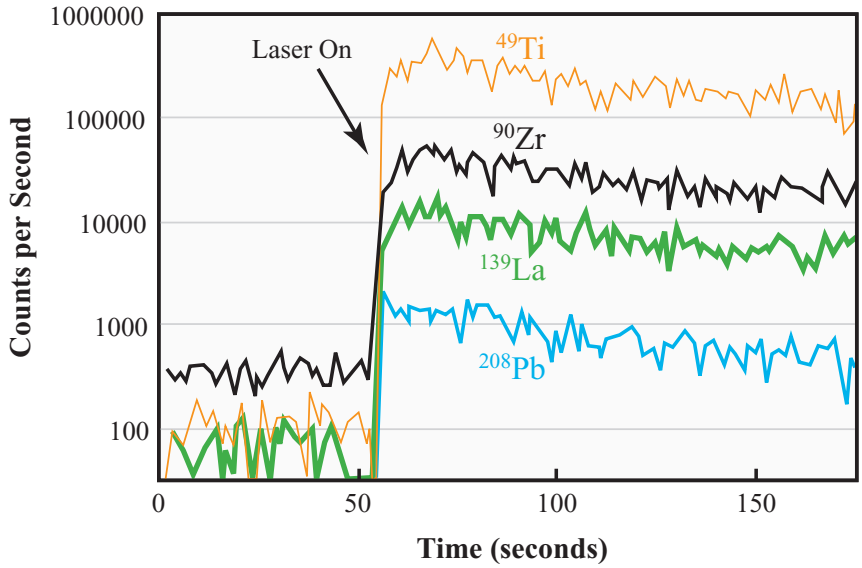

Figure 3. Time-resolved laser acquisition for selected elements in USGS standard BHVO-2G using the 213 nm Nd-YAG laser and VG PQ ExCell at Boston University. Backgound (laser off) signal is first 60 s, sample (laser on) is 60–180 s. Data are acquired by drilling a single 125 μm spot, 10 Hz repeat rate, 0.65 mJ/pulse beam energy, 0% beam expander and 20% iris. Pb background is off-scale, but averages 12 counts per second.

tion). Raw ICP-MS data were blank-subtracted, corrected for drift using an external drift correcting solution (analyzed every 5 samples), corrected for dilution weight, and calibrated using US Geological Survey (USGS), Geological Survey of Japan (GSJ), and internal laboratory standards. Standards used routinely in these analyses include K1919 and MAR (Lamont in-house standards for Kilauea 1919 and Mid-Atlantic Ridge basalts), DNC-1, W-2, BHVO-1, AGV-1, and BIR-1 (USGS), and JA-1 and JR-1 (GSJ) (Table 3). The GSJ standard basalt JB-3 was digesteded and analyzed as an unknown six times throughout the course of these analyses, demonstrating an average internal precision of 2% and an average difference from accepted values for JB-3 [*Imai et al.*, 1996] of <4% (Table 3). Calibration curves are linear ($r \geq 0.9990$), and reproducibility of replicate analyses is <2% rsd.

[11] Major and selected trace elements (Ni, Ba, Cr, Y, Cu, Zr, Sr) were measured using the Boston University Jobin-Yvon 170C ICP-AES, using data reduction protocols as described above for ICP-MS. Off-peak backgrounds were subtracted from trace elements with low signal/background ratios (Ni, Cr, Cu, Zr, Y) prior to data reduction. Table 1b shows ICP-AES operating conditions and instrument settings. To optimize analytical conditions for the alkalis (Na, K), we employ an increased sheath gas flow during alkali analysis that shifts the plasma alkali emission zone to the appropriate viewing position. Flushing the spectrometer with N_2 also permits sensitive and stable detection of P at 178 nm, which is otherwise obscured by an atmospheric interference. Elements measured on both instruments provide an internal check on instrumental accuracy and sample preparation yields. Agreement between the two techniques averages ≤5% for Sr, Ba and Zr (Figure 2). Six replicate digestions and analyses of GSJ standard JB-3 demonstrate an average internal precision of <1% and an average difference from accepted values for JB-3 [*Imai et al.*, 1996] of <2% (Table 3). Linear calibration curves yield $r \geq 0.9990$, replicate analyses are <2% rsd, and major element oxides sum to 100 ± 1 wt.%.

[12] Glasses from several intervals at Sites 801 and 1149 were analyzed for major elements by electron

Table 4. Comparison of Solution and LA-ICP-MS Data for Site 801 Glasses

	801C-23R-1-13-16			801C- 28R-2-118-122			801C-42R-2-116-120		
	Solution	LA	Difference, %	Solution	LA	Difference, %	Solution	LA	Difference, %
Li	***6.28***	***6.04***	***−4.1%***	**9.04**	***6.44***	***−40.5%***	***8.67***	***4.61***	***−88.2%***
Be	1.18			0.518			0.410		
Sc	46.5	46.2	−0.7%	43.2	45.4	5.0%	42.4	43.2	1.7%
V	394	431	8.5%	330	350	5.9%	281	284	1.1%
Cr	103	115	9.7%	223	229	2.8%	317	308	−2.8%
Co	44.8	45.7	1.9%	44.8	43.2	−3.7%	45.1	43.4	−3.9%
Ni	50.3	60.1	16.4%	79.2	61.1	−29.7%	91.1	75.1	−21.3%
Cu	72.8	70.4	−3.3%	75.4	71.4	−5.6%	86.3	73.3	−17.6%
Zn	130			88.7			77.1		
Ga	17.6			15.9			16.0		
Rb	***1.57***	***1.70***	***7.6%***	***2.27***	***1.10***	***−106.7%***	***2.70***	***0.485***	***−456.8%***
Sr	107	116	8.0%	111	104	−7.5%	138	120	−15.2%
Y	51.4	51.8	0.7%	37.8	37.5	−0.8%	28.9	30.4	5.0%
Zr	146	151	3.5%	107	106	−1.1%	85.4	86.6	1.4%
Nb	4.27	4.62	7.6%	3.06	3.11	1.6%	2.08	2.09	0.3%
Cs	0.0134			0.0306			0.0455		
Ba	***22.5***	***18.7***	***−20.1%***	***25.2***	***15.5***	***−62.3%***	***84.3***	***9.47***	***−790.5%***
La	4.63	5.03	8.0%	3.26	3.46	5.8%	2.48	2.86	13.3%
Ce	14.3	15.9	9.8%	10.6	11.1	5.0%	8.21	8.78	6.5%
Pr	2.59	2.70	4.1%	1.96	2.03	3.6%	1.53	1.62	5.3%
Nd	14.0	14.2	1.2%	10.2	11.0	7.0%	7.94	8.45	6.1%
Sm	4.95	5.10	2.9%	3.66	3.99	8.1%	2.83	2.83	0.2%
Eu	1.66	1.79	6.9%	1.28	1.32	3.4%	1.07	1.15	6.9%
Gd	7.00	7.37	5.0%	5.21	5.68	8.4%	4.02	4.48	10.3%
Tb	1.26	1.21	−4.1%	0.93	0.92	−1.3%	0.71	0.76	6.4%
Dy	8.35	7.96	−4.8%	6.20	6.37	2.6%	4.75	4.55	−4.5%
Ho	1.82	1.79	−1.6%	1.35	1.44	6.3%	1.02	1.12	8.9%
Er	5.22	4.97	−4.9%	3.87	4.08	5.1%	2.92	3.01	3.0%
Yb	5.27	4.90	−7.5%	3.79	3.89	2.4%	2.85	2.91	1.8%
Lu	0.835	0.795	−5.1%	0.600	0.626	4.2%	0.448	0.416	−7.8%
Hf	3.91	3.88	−0.9%	2.91	3.08	5.5%	2.23	2.31	3.5%
Ta	0.312	0.301	−3.7%	0.226	0.234	3.5%	0.157	0.152	−3.4%
Pb	0.416	0.474	12.4%	0.360	0.380	5.2%	0.325	0.284	−14.6%
Th	0.229	0.250	8.4%	0.172	0.179	4.3%	0.110	0.111	0.3%
U	***0.0894***	***0.0922***	***3.1%***	***0.136***	***0.0884***	***−54.3%***	***0.0500***	***0.0443***	***−12.9%***

Elements in ppm. Elements showing large differences between solution and laser are italicized. Differences are due to the incomplete separation of alteration phases from glass in dissolved separates, and laser data are prefereable for these elements. See text for analytical precision.

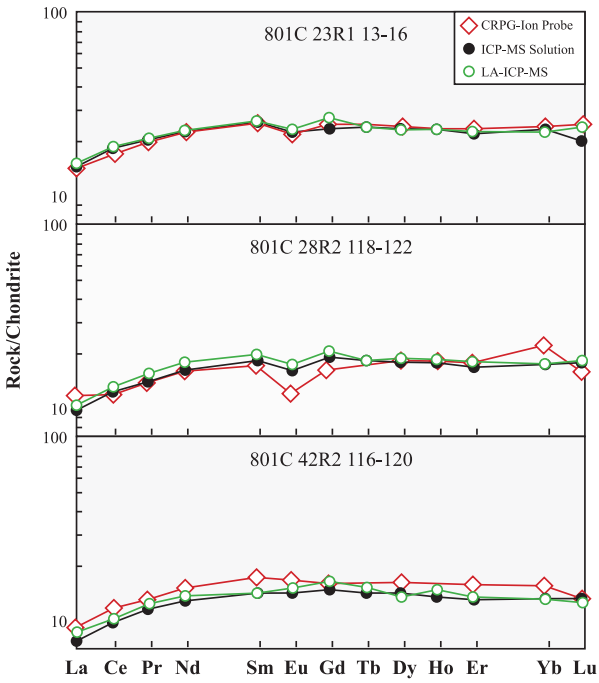

Figure 4. Comparison of chondrite-normalized REE patterns of Site 801 glasses measured using ion probe (CRPG), solution ICP-MS and LA-ICP-MS (BU). Chondrite values used for normalization are modified from *Nakamura* [1974] (Table 3).

microprobe [*Fisk and Kelley*, 2002] and for trace elements by laser-ablation (LA) ICP-MS using the Boston University Merchantek/VG MicroProbeII 213 nm Nd-YAG laser-ablation system. Glass chips were ablated using a 10 Hz repeat rate, 0.65 mJ/pulse beam energy (40% of maximum) and 125 μm spot size, achieved by setting the beam expander (collimation) to zero and the iris to 20% (additional settings in Table 1a). Drilling rates with these settings are 0.6–0.7 μm/second. Time-resolved data were acquired for each sample, first recording 60 s of background (laser off) and then ablating for 120 s (Figure 3). Laser focus is 200 μm below the sample surface, minimizing the fractionation of Pb from other elements. Lead-fractionation is a concern with many laser ablation microprobes [*Jeffries et al.*, 1998; *Horn et al.*, 2000; *Hirata and Nesbitt*, 1995], but in these analyses, Pb/Ti changed only 3% between the first and second 30 s of ablation. Intervals of ~30 s from each analysis are integrated, background-subtracted, and normalized to ^{49}Ti as an internal standard. Other laboratories routinely use ^{43}Ca as the internal standard [e.g., *Norman et al.*, 1996; *Dalpé and Baker*, 1995; *Eggins et al.*, 1998], but after testing both elements we find that Ti-normalization yields better calibration curves and reproducibility between spots. Trace element concentrations were calculated using a calibration of three USGS basaltic glass standards (BHVO-2G, BCR-2G, BIR-1G) ablated under the same conditions as the unknowns. We tested the NIST 612 glass standard with the USGS glasses but it fell consistently off the calibration curves, possibly due to ablation differences arising from composition (synthetic versus basalt) and color (clear versus brown). USGS glass values were determined using data from the USGS in combination with ICP-MS solution analyses on dissolved chips of the glasses (Table 3). Calibration curves were linear ($r \geq 0.9990$) and repeat laser analyses show reproducibility of <3% rsd for Sr, Nb, Y, and Th, and <10% rsd for Li, Ni, Rb, and U. We also dissolved chips of unknown glasses and analyzed the solutions by ICP-MS. Agreement between these two data sets is within 5–10% (Table 4) and agreement in the REE patterns is excellent (Figure 4). The two datasets differ in Li, Rb, Ba and U, not for analytical reasons, but because these elements are strongly affected by alteration. The differences reflect the superiority of the laser in avoiding altered domains that cannot be escaped in bulk digestions.

[13] As an external check on the ICP-MS data, we also analyzed glasses for trace elements on the Cameca IMS 3f ion microprobe at CRPG, Nancy, France. The analytical procedure for trace elements and REE follows *Fahey et al.* [1987]. A 15–20 nA, 10 kV O^- primary beam was focused to a 35 μm spot, leaving a ~50 μm pit in the gold-coated sample surface. Secondary ions were accelerated to 4500 eV and analyzed at a mass resolution of ~500 and an energy filtering at −60 ± 10 V. Low filtering energy is advantageous because it keeps counting rates high while removing complex molecular interferences. The different atomic masses were measured by peak switching, with counting times of 5–10 s on each peak and waiting time of 1 second. Successive measurements were acquired over 120 min on one sample position. Remaining interferences on REE (LREE and Ba

10.1029/2002GC000435

Table 5. Comparison of LA-ICP-MS and Ion Probe Data for Site 801 and 1149 Glasses[a]

	801C-12R-1-57-61			801C-23R-1-13-16			801C-28R-2-118-122			801C-42R-2-116-120			801C-46R-1-45-51			1149D-8R-1-55-58		
Lab	CRPG	LA	Difference, %	CRPG	LA	Difference, %	CRPG	LA	Difference, %	CRPG	LA	Difference, %	CRPG	LA	Difference, %	CRPG	LA	Difference, %
Sc	43.0	47.3	−8.9%	42.2	46.2	−8.7%	41.1	45.4	−9.5%	39.1	43.2	−9.4%	42.5	46.6	−8.9%	39.8	43.6	−8.7%
V	394	453	−13.1%	346	431	−19.6%	311	350	−11.3%	262	284	−7.7%	341	406	−16.0%	300	347	−13.5%
Sr	170	130	30.7%	126	116	8.5%	98.1	103.7	−5.3%	135	120	12.6%	123	117	5.1%	118	115	2.5%
Y	52.5	59.5	−11.8%	49.9	51.8	−3.6%	34.7	37.5	−7.3%	31.0	30.4	1.9%	46.5	48.0	−3.1%	38.8	41.6	−6.7%
Zr	153	178	−13.6%	140	151	−7.3%	94.9	106.1	−10.6%	83.9	86.6	−3.1%	128	139	−8.0%	103	125	−17.1%
Nb	4.45	4.27	4.2%	4.13	4.62	−10.7%	2.69	3.11	−13.3%	2.18	2.09	4.4%	3.71	3.78	−1.7%	3.21	4.04	−20.5%
Ba	34.7	15.8	119.2%	18.7	18.7	−0.1%	14.6	15.5	−6.3%	9.9	9.5	4.4%	17.2	17.3	−0.2%	14.8	16.7	−11.6%
La	4.97	5.34	−7.0%	4.69	5.03	−6.8%	3.80	3.46	9.7%	2.99	2.86	4.5%	4.03	4.58	−11.9%	3.91	4.51	−13.3%
Ce	16.3	17.2	−5.0%	15.5	15.9	−2.5%	10.1	11.1	−9.4%	9.9	8.8	12.3%	14.2	13.9	2.4%	12.2	13.6	−10.4%
Pr	2.84	3.07	−7.4%	2.64	2.70	−2.5%	1.78	2.03	−12.4%	1.68	1.62	3.8%	2.50	2.44	2.4%	2.03	2.35	−13.8%
Nd	15.6	15.7	−0.4%	14.3	14.2	0.9%	10.2	11.0	−7.3%	9.33	8.45	10.4%	13.7	13.4	2.4%	11.2	12.3	−8.8%
Sm	5.77	6.13	−6.0%	5.26	5.10	3.1%	3.41	3.99	−14.6%	3.45	2.83	21.8%	5.06	4.87	3.9%	4.24	4.49	−5.5%
Eu	1.82	2.02	−9.7%	1.74	1.79	−2.6%	0.93	1.32	−29.5%	1.26	1.15	9.9%	1.56	1.58	−1.2%	1.45	1.53	−4.9%
Gd	7.07	8.31	−14.9%	6.44	7.37	−12.7%	4.44	5.68	−21.8%	4.21	4.48	−6.0%	6.71	6.77	−0.8%	5.19	5.86	−11.4%
Dy	9.05	9.14	−1.0%	8.28	7.96	3.9%	6.01	6.37	−5.6%	5.49	4.55	20.6%	8.23	7.56	8.8%	6.84	6.75	1.4%
Er	5.89	5.71	3.1%	5.08	4.97	2.2%	4.15	4.08	1.7%	3.50	3.01	16.5%	5.21	4.55	14.6%	4.34	4.16	4.2%
Yb	6.28	5.58	12.5%	5.18	4.90	5.7%	4.80	3.89	23.6%	3.35	2.91	15.3%	5.30	4.47	18.6%	4.44	4.03	10.1%
Lu	0.775	0.885	−12.4%	0.673	0.795	−15.3%	0.541	0.626	−13.7%	0.434	0.416	4.2%	0.696	0.692	0.6%	0.551	0.687	−19.8%

[a] Elements in ppm. CRPG are data collected by ion probe at CRPG, Nancy, France. LA are data acquired by laser-ablation ICP-MS at Boston University. See text for analytical precision.

Table 6 (Representative Sample). Major and Trace Element Analyses of Site 801 and 1149 Basement Samples. [The full Table 6 is available in the HTML version of this article at http://www.g-cubed.org.]

	801B-37R-1		801B-39R-1		801B-40R-1	801B-41R-1		801B-41R-2	801B-42R-2	801B-43R-1	
Interval (cm)	22–27	36–38	8–10	25–27	46–50	26–30	66–70	74–79	100–102	61–66	132–135
Description	chert	alt. basalt	chert	chert	basalt	basalt	basalt + cc vein	basalt	basalt + cc vein	basalt + cc vein	basalt
Depth (mbsf)	461.72	461.86	470.78	470.95	477.36	483.26	483.66	485.24	489.68	492.81	493.52
ICP-AES											
SiO_2	97.41	59.69	92.77	96.60	53.06	47.92	46.55	48.70	40.35	45.71	47.30
TiO_2	0.0256	2.67	0.07	0.0517	3.40	3.17	3.12	3.03	2.32	2.47	2.42
Al_2O_3	1.26	19.57	4.12	1.06	18.63	16.76	16.46	16.82	13.48	13.81	13.54
Fe_2O_3	1.72	3.91	1.93	1.99	8.32	10.66	10.40	10.90	10.04	12.24	12.51
MnO	0.0358	0.191	0.212	0.116	0.0800	0.154	0.222	0.171	0.368	0.173	0.153
MgO	0.142	2.65	0.195	0.0957	2.84	5.18	5.32	5.10	8.57	11.30	11.16
CaO	0.0788	1.40	0.158	0.122	3.34	8.61	10.67	8.95	19.78	8.36	6.85
Na_2O	0.0759	2.34	0.108	0.139	2.41	3.53	3.88	3.46	2.77	3.13	3.22
K_2O	0.191	7.30	0.331	0.237	6.21	2.40	2.19	2.83	1.59	1.66	1.61
P_2O_5	0.0180	0.446	0.0762	0.0464	0.785	0.690	0.706	0.691	0.527	0.565	0.512
Total	100.96	100.15	99.97	100.46	99.07	99.07	99.52	100.65	99.79	99.43	99.28
LOI	0.36	2.83	1.01	0.00	6.04	2.89	7.51	5.62	15.48	5.85	5.74
Sr	4.01	134	4.92	7.08	115	544	551	531	502	592	376
Ba	19.2	581	241	222	475	451	464	428	311	421	421
Ni	49.2	57.6	6.40	7.02	70.2	40.7	38.9	40.7	46.9	272	–
Cr	0.885	141	4.12	2.50	102	82.3	68.1	98.4	115	253	316
Cu	15.4	283	24.0	25.1	7.94	28.8	18.6	34.4	50.8	24.7	35.5
Zr	12.6	169	14.9	16.5	237	310	298	282	212	232	235
Y	–	31.1	9.72	4.95	32.3	32.9	34.6	32.7	31.9	25.1	23.8
ICP-MS											
Li		35.6				24.0		23.6			25.9
Be		1.13				2.60		2.59			2.10
Sc		25.0				23.4		22.6			19.2
V		107				232		225			173
Cr		132				77.6		90.2			270

HT, hydrothermal; alt, altered; cc, calcite; IFM, interflow material; celad, celadonite: sap, saponite; FeOx, Fe-oxyhydroxide. Blank space indicates element not measured; dashes indicate below detection limits; asterisks indicate measured at University of Kansas ICP-MS lab; cross indicates measured at both University of Kansas and Boston University labs. ICP-AES data relative to ignited powder, ICP-MS data relative to non-ignited powder. Oxides and LOI in weight percent, all other elements in ppm. See text for analytical precision. Metadata for each sample are available in Table B (see auxiliary material).

Table 7. Major and Trace Element Analyses of Site 801 Composite Samples[a]

	801-TAB-0-50			801-MORB-0-110			801-MORB-110-220			801-MORB-220-420			801	801
Type	FLO	VCL	All	FLO	VCL	All	FLO	VCL	All	FLO	VCL	All	SUPER	SED
Depth (mbsf)	487.00	487.00	487.00	575.00	575.00	575.00	680.50	680.50	680.50	839.50	839.50	839.50		
ICP-AES														
SiO_2	48.26	59.95	51.93	46.71	51.78	47.85	48.06	53.11	49.65	49.70	51.00	49.67	49.23	64.61
TiO_2	2.84	1.43	2.40	1.66	0.411	1.32	2.09	0.969	1.82	2.04	1.71	1.94	1.70	0.191
Al_2O_3	16.29	8.45	14.50	15.06	5.46	11.97	14.02	7.16	12.22	12.70	10.97	12.38	12.05	2.52
Fe_2O_3	9.94	7.14	9.28	12.33	13.44	12.72	13.57	13.31	13.73	14.63	15.17	14.56	13.72	9.73
MnO	0.297	0.662	0.406	0.253	0.322	0.270	0.215	0.231	0.222	0.216	0.175	0.201	0.226	0.531
MgO	5.77	5.71	5.70	5.31	4.43	5.20	6.52	5.96	6.52	6.63	7.47	6.84	6.22	2.66
CaO	8.65	12.69	9.88	15.35	21.66	17.32	12.36	17.22	13.76	10.88	9.89	10.58	13.03	19.33
Na_2O	3.48	1.62	2.90	2.53	0.717	1.95	2.66	1.40	2.31	2.63	2.26	2.49	2.30	0.201
K_2O	3.66	1.55	3.24	0.790	1.389	1.00	0.135	0.953	0.389	0.390	0.914	0.566	0.620	0.716
P_2O_5	0.620	0.329	0.548	0.152	0.0780	0.127	0.196	0.111	0.166	0.199	0.168	0.187	0.168	0.099
Total	99.81	99.53	100.79	100.15	99.69	99.74	99.83	100.42	100.78	100.00	99.72	99.41	99.25	100.59
LOI	7.85	14.03	10.08	9.51	19.11	11.56	3.05	12.47	5.86	2.46	5.99	3.48	6.31	16.97
ICP-MS														
Li	22.2	20.7	21.5	12.3	14.9	13.6	10.8	23.4	15.5	11.2	16.5	13.3	14.1	14.0
Be	2.30	1.62	2.07	0.49	0.246	0.430	0.644	0.412	0.607	0.683	0.513	0.661	0.584	0.396
Sc	18.1	11.3	15.9	40.1	16.5	33.2	43.1	19.7	36.9	41.8	30.4	39.4	37.4	12.3
V	175	99	150	316	99.0	251	395	168	337	399	290	376	338	50.8
Cr	89.9	38.1	76.4	182	55.9	145	132	57.4	113	105	74.1	97.8	114	13.1
Co	28.4	15.2	24.5	41.4	16.4	34.6	44.9	19.0	38.2	40.6	22.7	37.1	36.7	8.76
Ni	73.2	33.4	61.0	78.1	40.3	68.4	57.4	25.9	48.7	48.7	32.1	45.7	52.7	23.5
Cu	48.3	28.1	41.5	65.3	26.8	55.3	66.7	33.4	58.0	61.5	43.9	55.8	57.3	7.48
Zn	79.5	54.0	69.9	84.4	32.1	69.4	101	35.7	84.6	105	77.5	97.7	88.5	25.3
Ga	21.0	11.2	17.5	15.7	5.00	12.4	17.5	8.54	15.4	17.6	13.2	16.6	15.6	2.55
Rb	51.4	24.8	43.5	12.0	28.8	18.0	2.74	21.2	9.20	10.4	20.0	13.6	13.7	12.5
Sr	372	221	324	128	75.8	113	117	65.9	105	111	84.8	105	109	63.5

Table 7. (continued)

	801-TAB-0-50			801-MORB-0-110			801-MORB-110-220			801-MORB-220-420			801	801
Type	FLO	VCL	All	FLO	VCL	All	FLO	VCL	All	FLO	VCL	All	SUPER	SED
Y	29.5	22.7	27.2	36.7	17.8	31.6	45.6	23.0	40.2	47.6	36.5	45.4	40.7	13.6
Zr	251	156	221	97.8	32.0	79.0	133	58.7	114	133	103	127	112	37.9
Nb	49.6	22.1	40.3	2.28	0.491	1.76	3.65	1.68	3.11	3.65	2.92	3.36	2.89	2.07
Cs	0.713	0.352	0.716	0.221	0.380	0.343	0.133	0.344	0.248	0.259	0.465	0.370	0.317	0.265
Ba	442	257	383	14.6	12.7	14.9	10.5	48.0	20.8	12.3	12.8	12.8	15.6	78.5
La	25.8	16.5	22.2	2.83	1.43	2.42	3.74	2.05	3.38	4.03	3.50	3.79	3.40	3.41
Ce	59.8	35.4	51.9	9.84	3.16	7.94	13.5	5.79	11.5	13.9	10.6	13.1	11.4	5.73
Pr	7.76	4.85	6.81	1.82	0.660	1.48	2.45	1.05	2.06	2.55	1.95	2.34	2.06	1.03
Nd	30.8	19.9	27.0	10.1	3.51	8.21	13.2	5.50	11.3	13.5	10.3	12.7	11.3	4.58
Sm	6.65	4.39	5.87	3.61	1.22	2.91	4.62	1.88	3.95	4.71	3.59	4.46	3.95	1.19
Eu	2.20	1.40	1.92	1.26	0.414	1.02	1.56	0.651	1.33	1.57	1.19	1.48	1.34	0.381
Gd	6.68	4.58	5.95	5.08	1.90	4.17	6.39	2.73	5.50	6.53	5.01	6.21	5.55	1.58
Tb	1.06	0.718	0.944	0.931	0.353	0.764	1.16	0.491	1.00	1.20	0.901	1.13	1.01	0.270
Dy	5.83	3.96	5.17	6.05	2.45	5.00	7.48	3.28	6.46	7.72	5.83	7.30	6.56	1.74
Ho	1.08	0.744	0.959	1.31	0.580	1.10	1.61	0.753	1.41	1.68	1.29	1.59	1.43	0.392
Er	2.87	1.98	2.55	3.74	1.73	3.17	4.59	2.21	4.04	4.80	3.64	4.53	4.09	1.13
Yb	2.47	1.74	2.21	3.62	1.82	3.11	4.48	2.36	3.99	4.65	3.59	4.41	4.02	1.14
Lu	0.377	0.270	0.337	0.565	0.293	0.489	0.700	0.387	0.633	0.732	0.560	0.696	0.636	0.191
Hf	5.70	2.88	4.73	2.74	0.74	2.14	3.64	1.49	3.09	3.68	2.81	3.47	3.07	0.555
Ta	2.95	1.34	2.42	0.169	0.0459	0.133	0.255	0.120	0.219	0.255	0.216	0.242	0.210	0.138
Pb	1.97	1.30	1.74	0.395	0.142	0.331	0.541	0.203	0.492	0.465	0.307	0.445	0.437	0.560
Th	3.01	1.45	2.44	0.143	0.0606	0.119	0.207	0.095	0.178	0.204	0.154	0.191	0.173	0.248
U	1.05	0.823	0.922	0.344	0.390	0.358	0.356	0.337	0.363	0.385	0.469	0.405	0.390	0.347

[a] TAB, top alkali basalt; MORB, mid-ocean ridge tholeiite; FLO, less altered basaltic flows; VCL, highly altered breccias (volcaniclastics); IFM, interflow material. Super, all Site 801 tholeiite; Sed, all Site 801 IFM. ICP-AES data relative to ignited powder, ICP-MS data relative to non-ignited powder. Oxides and LOI in weight percent, all other elements in ppm. See text for analytical precision. Recipes for composite mixtures are available in data table A (see auxiliary material).

Table 8. LA-ICP-MS Trace Element Analyses of Site 801 and 1149 Glasses[a]

	801C-12R-1-57-61	801C-23R-1-13-16	801C-28R-2-118-122	801C-42R-2-116-120	801C-46R-1-45-51	1149B-31R-1-108	1149D-8R-2-5558
Description	glass	glass	glass	glass	glass	glass	glass
Depth (mbsf)	602.87	682.03	731.22	862.37	898.45	331.35	427.04
LA-ICP-MS							
Li	7.93	6.04	6.44	4.61	7.19	6.99	6.55
Sc	47.3	46.2	45.4	43.2	46.6	43.6	45.2
V	453	431	350	284	406	347	354
Cr	78.0	115	229	308	133	126	241
Co	48.0	45.7	43.2	43.4	46.1	44.0	45.8
Ni	35.6	60.1	61.1	75.1	58.8	60.1	74.2
Cu	80.4	70.4	71.4	73.3	76.0	75.1	80.7
Rb	1.53	1.70	1.10	0.48	1.46	1.42	1.12
Sr	130	116	104	120	117	115	113
Y	59.5	51.8	37.5	30.4	48.0	41.6	40.1
Zr	178	151	106	87	139	125	106
Nb	4.27	4.62	3.11	2.09	3.78	4.04	3.03
Ba	15.8	18.7	15.5	9.47	17.3	16.7	13.2
La	5.34	5.03	3.46	2.86	4.58	4.51	3.49
Ce	17.2	15.9	11.1	8.78	13.9	13.6	11.1
Pr	3.07	2.70	2.03	1.62	2.44	2.35	1.95
Nd	15.7	14.2	11.0	8.45	13.4	12.3	10.6
Sm	6.13	5.10	3.99	2.83	4.87	4.49	3.66
Eu	2.02	1.79	1.32	1.15	1.58	1.53	1.34
Gd	8.31	7.37	5.68	4.48	6.77	5.86	5.51
Tb	1.40	1.21	0.921	0.763	1.11	1.05	0.926
Dy	9.14	7.96	6.37	4.55	7.56	6.75	6.64
Ho	2.05	1.79	1.44	1.12	1.66	1.47	1.46
Er	5.71	4.97	4.08	3.01	4.55	4.16	4.16
Yb	5.58	4.90	3.89	2.91	4.47	4.03	3.90
Lu	0.885	0.795	0.626	0.416	0.692	0.687	0.626
Hf	4.36	3.88	3.08	2.31	3.61	3.17	2.93
Ta	0.306	0.301	0.234	0.152	0.260	0.267	0.205
Pb	0.492	0.474	0.380	0.284	0.438	0.457	0.390
Th	0.209	0.250	0.179	0.111	0.200	0.229	0.170
U	0.0803	0.0922	0.0884	0.0443	0.0716	0.0838	0.0545

[a] Elements in ppm. See text for analytical precision. Major element data available from *Fisk and Kelley* [2002].

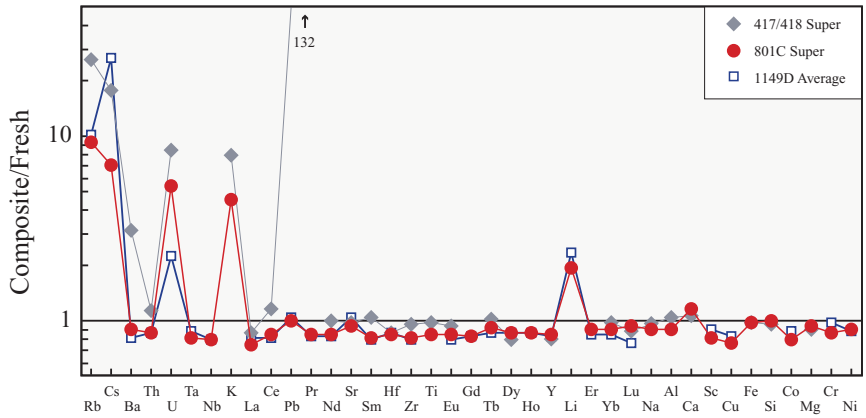

Figure 5. Super composite samples of upper 500 m of altered oceanic crust at ODP Sites 417/418 (118 Ma, W. Altantic) [*Staudigel et al.*, 1996] and 801 (170 Ma, W. Pacific; Table 7), as well as a simple average of Site 1149D NMORB (upper 100 m; Table 6), normalized to "fresh" igneous compositions. Site 801 and 1149 data are normalized to glasses (801C-46R1-45-51 and 1149D-8R2-55-58), and 417/418 data [*Staudigel et al.*, 1996] are normalized to a minimally altered whole rock (418A-19R6-5-7) [*Emmermann and Puchelt*, 1980]. Note extremely high Pb in 417/418 composite, which is due to catastrophic Pb contamination in these samples. Sequence of elements adopted from *Hofmann* [1988].

oxides interfering with HREE) are removed by deconvolution techniques [*Fahey et al.*, 1987], after measuring 31 atomic masses from 138 to 180. Secondary ion currents are normalized to Si, and secondary yields relative to Si determined on standards. Standards for the ion microprobe included synthetic glasses NBS 613 and KL2-G [*Jochum et al.*, 2000]. Agreement between the ICP-MS and ion probe techniques is ~10% or better (Table 5), and the three data sets (ICP-MS solution, laser, and ion probe) compare well and demonstrate the high quality of data generated by the relatively new laser-ablation technique.

4. Results and Discussion

[14] Analytical results are presented in Tables 6–8. As a first-order evaluation of net alteration fluxes, we normalize the 801 "super composite" (Table 7; bulk Site 801 tholeiitic section) and a simple average of the Site 1149D NMORB (Table 6) to glasses from the same sites (Figure 5), effectively removing the igneous contribution and emphasizing elements affected by alteration. Elements enriched over 100% in AOC are the alkalis (Li, K, Rb, Cs) and U, those enriched 5–15% are Ca, Pb, Si and Fe. All other elements appear unaffected by alteration, except for a 15–20% shift in abundance due to dilution by $CaCO_3$ and H_2O. Alkali and/or U-enrichment have been documented at Sites 417/418 and 504B [*Staudigel et al.*, 1996; *Alt et al.*, 1996], but Site 417/418 shows Ba-enrichment that is absent at Site 801, and the 801 composite has clearly avoided the catastrophic Pb-contamination suffered by the 417/418 samples. *Kelley et al.* [2000, manuscript in preparation, 2003] explore the global implications of U-Th-Pb fractionations during seafloor alteration. Both the 417/418 and 801 super composites show bulk Ca-enrichment and no change in Mg, contradicting sedimentary pore water profiles interpreted to indicate Ca-Mg exchange as calcic plagioclase weathering forms magnesian saponite clay [*Plank et al.*, 2000].

[15] Comparing U data from the downhole natural gamma logging tool (NGT) to data acquired on discrete samples by ICP-MS (Figure 6a) reveals a strong correlation. Using adjusted sample depths within the borehole [*Barr et al.*, 2002; *Révillon et al.*, 2002] and matching these to depths on the NGT logs provides a direct means of comparing the two data sets. When plotted against each other (Figure 6b), most of the data fall close to a 1:1 line. The logs are an average of 11% different from the ICP-MS data over a concentration range of 0.10–1.73 ppm. Bulk U determined for Site 801 by averaging the logging data in the tholeiites (527–

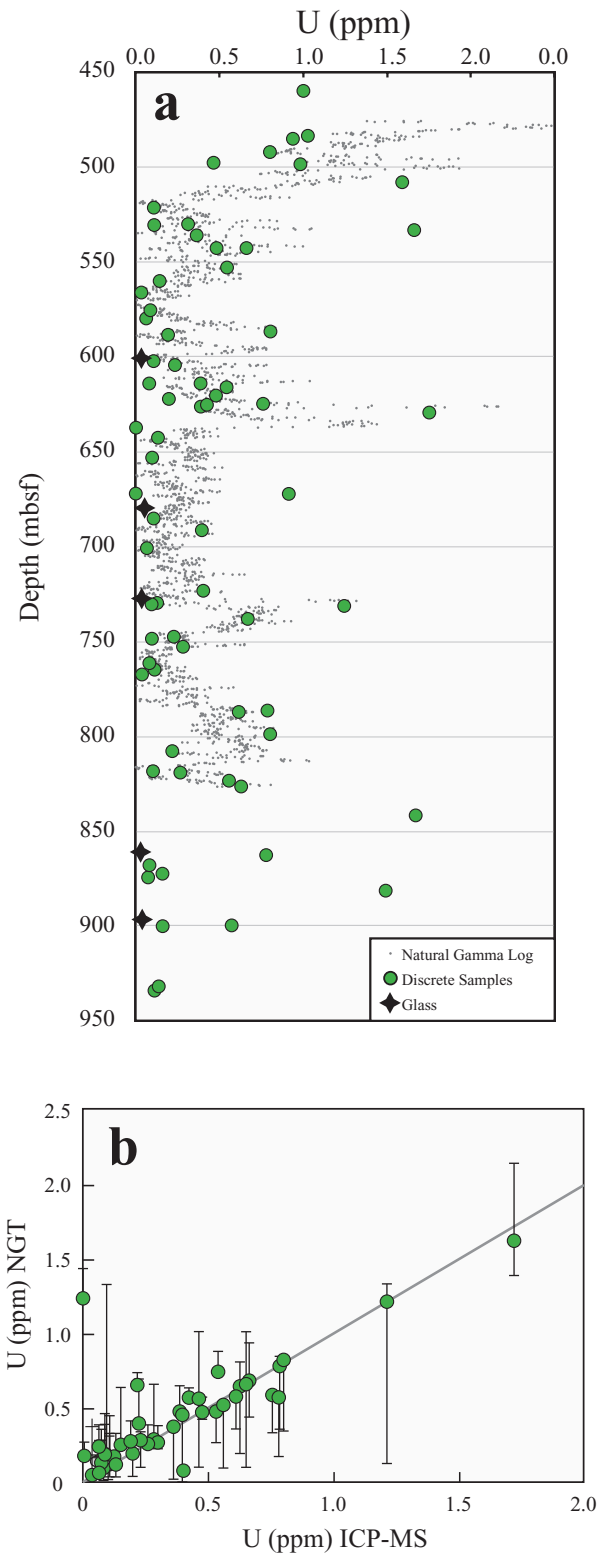

826 mbsf) is 0.37 ppm, while bulk U from the "super-composite" is 0.39 ppm (Table 7). *Révillon et al.* [2002] performed a detailed evaluation of K_2O and U logging data accuracy by estimating the proportions of discrete sample lithologies in the core using FMS logs, then calculating the bulk composition of the core using these proportions and comparing this to the K_2O and U logs. They conclude that scaling discrete samples to their log-derived proportions yields a bulk K_2O of 0.51 wt.% and U of 0.39 ppm, while the NGT data average 0.47 wt.% K_2O and 0.42 ppm U. These comparisons show the logging data to be a reliable means of identifying enriched domains within the crust and estimating its bulk composition.

[16] Analyzing discrete samples, however, is advantageous because their systematics may reveal alteration mechanisms. The largest effect of sea-floor alteration is to increase the alkali elements and U. Geochemical and mineralogical data show that alkalis are largely associated with celadonite, a K-rich clay mineral. Natural gamma radiation measurements of the core at Site 801 show three distinct zones of K-enrichment [*Plank et al.*, 2000], rather than the expected decrease with depth observed at Sites 504B and 417/418. These zones coincide with major lithologic features (breccia, upper and lower hydrothermal deposits) controlling fluid flow through the crust. Uranium is also enriched in specific zones, but these are unrelated to alkali enrichment. Uranium-enrichment is apparently controlled by two distinct processes: calcite formation and redox reactions. *Staudigel et al.* [1996] showed a positive correlation between CO_2 and U in the Site 417/418 composites, but

Figure 6. (opposite) (a) Correspondence between uranium NGT logging data and ICP-MS analyses of discrete samples versus depth at ODP Site 801. (b) NGT data versus ICP-MS data agree on average within 11%. Circles are placed on the closest log-determined concentrations to each discrete sample within the depth uncertainty, bars show the full range of log U values within the depth uncertainty [*Barr et al.*, 2002; *Révillon et al.*, 2002]. Gray line is 1:1 correlation. Samples deviating significantly from the 1:1 line are small-scale features that are averaged by the 15 cm footprint of the logging tool [*Révillon et al.*, 2002].

data from discrete alteration domains at Site 801 [*Farr et al.*, 2001] shows U to be concentrated in certain generations of calcite and in haloes proximal to veins.

Acknowledgments

[17] We thank the ODP Leg 185 shipboard scientific party, especially J. Alt, for enabling and assisting the sampling of these precious cores, as well as the laboratory technicians and crew of the JOIDES *Resolution*, without whom this work would have been impossible. Thanks to R. Murray, K. Kryc, L. Wincze and P. Burger at Boston University for sharing their invaluable expertise with the ICP-AES. Thanks also to D. Gravatt and C. Spies for assistance with the ICP-MS at the University of Kansas. We appreciate the thoughtful reviews and comments of B. Peucker-Ehrenbrink and W. White. This material is based upon work supported under a JOI/USSSP research grant and a National Science Foundation Graduate Fellowship.

References

Alt, J. C., and D. Teagle, The uptake of carbon during alteration of ocean crust, *Geochim. Cosmochim. Acta*, *63*, 1527–1535, 1999.

Alt, J. C., et al., Hydrothermal alteration of a section of upper oceanic crust in the eastern equatorial Pacific: A synthesis of results from Site 504 (DSDP Legs 69, 70, and 83, and ODP Legs 111, 137, 140, and 148), *Proc. Ocean Drill. Program Sci. Results*, *148*, 417–434, 1996.

Bach, W., et al., The geochemical consequences of late-stage low-grade alteration of lower ocean crust at the SW Indian Ridge: Results from ODP Hole 735B (Leg 176), *Geochim. Cosmochim. Acta*, *65*, 3267–3287, 2001.

Balzer, V., The late Miocene history of sediment subduction and recycling as recorded in the Nicaraguan volcanic arc, M.S. thesis, Univ. of Kan., Lawrence, 1999.

Barr, S. R., S. Révillon, T. S. Brewer, P. K. Harvey, and J. Tarney, Determining the inputs to the Mariana Subduction Factory: Using core-log integration to reconstruct basement lithology at ODP Hole 801C, *Geochem. Geophys. Geosyst.*, *3*(11), 8901, doi:10.1029/2001GC000255, 2002.

Bartolini, A., and R. L. Larson, Pacific microplate and the Pangea supercontinent in the Early to Middle Jurassic, *Geology*, *29*, 735–738, 2001.

Cande, S. C., and D. V. Kent, Revised calibration of the geomagnetic polarity timescale for the late Cretaceous and Cenozoic, *J. Geophys. Res.*, *100*, 6093–6095, 1995.

Castillo, P. R., P. A. Floyd, C. France-Lanord, and J. C. Alt, Data Report: Summary of geochemical data for Leg 129 igneous rocks, *Proc. Ocean Drill. Program Sci. Results*, *129*, 653–669, 1992.

Chauvel, C., and C. Hémond, Melting of a complete section of recycled oceanic crust: Trace element and Pb isotopic evidence from Iceland, *Geochem. Geophys. Geosys.*, *1*, Paper number 1999GC000002, 2000.

Cheatham, M. M., W. F. Sangrey, and W. M. White, Sources of error in external calibration ICP-MS analysis of geological samples and an improved non-linear drift correction procedure, *Spectrochimica Acta, Part B*, *48*, E487–E506, 1993.

Dalpé, C., and D. R. Baker, Synchrotron X-ray fluorescence and laser-ablation ICP-MS microprobes: Useful instruments for analysis of experimental run-products, *Can. Mineral.*, *33*, 481–498, 1995.

Eggins, S., et al., A simple method for the precise determination of >40 trace elements in geological samples by ICPMS using enriched isotope internal standardisation, *Chem. Geol.*, *134*, 311–326, 1997.

Eggins, S., R. L. Rudnick, and W. F. McDonough, The composition of peridotites and their minerals: A laser-ablation ICP-MS study, *Earth Planet. Sci. Lett.*, *154*, 53–71, 1998.

Elliott, T., T. Plank, A. Zindler, W. M. White, and B. Bourdon, Element transport from slab to volcanic front at the Mariana arc, *J. Geophys. Res.*, *102*, 14,991–15,019, 1997.

Emmermann, R., and H. Puchelt, Major and trace element chemistry of basalts from holes 417D and 418A, Deep Sea Drilling Project Legs 51–53, *Init. Rep. Deep Sea Drill. Proj.*, *51–53*, 987–1000, 1980.

Fahey, A. J., J. N. Goswami, K. D. McKeegan, and E. Zinner, 26Al, 244Pu, 50Ti, REE, and trace element abundances in hibonite grains from CM and CV meteorites, *Geochim. Cosmochim. Acta*, *51*, 329–350, 1987.

Farr, L., T. Plank, and K. A. Kelley, U Mineral Hosts and Enrichment Processes in Altered Oceanic Crust, *Eos Trans. AGU*, *82*(47), Fall Meet. Suppl., F1147, 2001.

Fisk, M., and K. A. Kelley, Probing the Pacific's Oldest MORB Glass: Mantle Chemistry and Melting Conditions during the Birth of the Pacific Plate, *Earth Planet. Sci. Lett.*, *202*, 741–752, 2002.

Hart, S. R., and H. Staudigel, Isotopic characterization and identification of recycled components, in *Crust/Mantle Recycling at Convergence Zones*, edited by S. R. Hart and L. Gülen, pp. 15–28, Kluwer Acad., Norwell, Mass., 1989.

Hirata, T., and R. W. Nesbitt, U-Pb isotope geochronology of zircon: evaluation of the laser probe-inductively coupled plasma spectrometry technique, *Geochim. Cosmochim. Acta*, *59*, 2491–2500, 1995.

Hofmann, A. W., Chemical differentiation of the Earth: the relationship between mantle, continental crust, and oceanic crust, *Earth Planet. Sci. Lett.*, *90*, 297–314, 1988.

Hofmann, A. W., and W. M. White, Mantle plumes from ancient oceanic crust, *Earth Planet. Sci. Lett.*, *57*, 421–436, 1982.

Horn, I., R. L. Rudnick, and W. F. McDonough, Precise elemental and isotope ratio determination by simultaneous solution nebulization and laser ablation-ICP-MS: application to U-Pb geochronology, *Chem. Geol.*, *164*, 281–301, 2000.

Imai, N., H. Sakuramachi, S. Terashima, S. Itoh, and A. Ando, Database on Internet for Geological Survey of Japan geochemical reference samples, *Geostand. Newsl.*, *20*(2), 161–164, 1996.

Ishikawa, T., and E. Nakamura, Origin of the slab component in arc lavas from across-arc variation of B and Pb isotopes, *Nature*, *370*, 205–208, 1994.

Jarrard, R. D., Relations Among Subduction Parameters, *J. Geophys. Res.*, *24*, 217–284, 1986.

Jeffries, T. E., S. E. Jackson, and H. P. Longerich, Application of a frequency quintupled Nd:YAG source (wavelength = 213 nm) for laser ablation ICP-MS analysis of minerals, *J. Anal. At. Spectrom.*, *13*, 935–940, 1998.

Jenner, G. A., H. P. Longerich, S. E. Jackson, and B. J. Fryer, ICP-MS - A powerful tool for high-precision trace-element analysis in earth sciences: Evidence from analysis of U.S.G.S. selected reference samples, *Chem. Geol.*, *83*, 133–148, 1990.

Jochum, K. P., M. Rehkamper, and H. M. Seufert, Trace elements analysis of basalt BIR-1 by ID-SSMS HPLC and LIMS, *Geostand. Newsl.*, *18*, 43–51, 1994.

Jochum, K. P., et al., The preparation and preliminary characterisation of eight geological MPI-DING reference glasses for in-situ microanalysis, *Geostand. Newsl.*, *24*, 87–133, 2000.

Johnson, M. C., and T. Plank, Dehydration and melting experiments constrain the fate of subducted sediments, *Geochem. Geophys. Geosyst.*, *1*, Paper number 1999GC000014, 1999.

Kelley, K. A., et al., Subduction cycling of altered oceanic crust: U, Th and Pb Budgets, *Eos Trans. AGU*, *81*(48), Fall Meet. Suppl., F1354, 2000.

Klein, E. M., C. H. Langmuir, and H. Staudigel, Geochemistry of basalts from the southeast Indian Ridge, 115°E–138°E, *J. Geophys. Res.*, *96*, 2089–2107, 1991.

Lancelot, Y. P., et al., *Proceedings of the Ocean Drilling Program, Initial Reports*, vol. 129, Ocean Drill. Program, College Station, Tex., 1990.

Mattinson, J. M., Preparation of hydrofluoric, hydrochloric, and nitric acids at ultralow lead levels, *Anal. Chem.*, *44*, 1715–1716, 1972.

Miller, D. M., C. H. Langmuir, S. L. Goldstein, and A. L. Franks, The importance of parental magma composition to calc-alkaline and tholeiitic evolution: Evidence from Umnak Island in the Aleutians, *J. Geophys. Res.*, *97*, 321–343, 1992.

Miller, D. M., S. L. Goldstein, and C. H. Langmuir, Cerium/lead and lead isotope ratios in arc magmas and the enrichment of lead in the continents, *Nature*, *368*, 514–519, 1994.

Nakamura, N., Determination of REE, Ba, Fe, Mg, Na and K in carbonaceous and ordinary chondrites, *Geochim. Cosmochim. Acta*, *38*, 757–775, 1974.

Norman, M. D., N. J. Pearson, A. Sharma, and W. L. Griffin, Quantitative Analysis of Trace Elements in Geological Materials by Laser Ablation ICPMS: Instrumental Operating Conditions and Calibration Values of NIST Glasses, *Geostand. Newsl.*, *20*, 247–261, 1996.

Plank, T., and J. N. Ludden, Geochemistry of sediments in the Argo abyssal plain at Site 765: A continental margin reference section for sediment recycling in subduction zones, *Proc. Ocean Drill. Program Sci. Results*, *123*, 167–189, 1992.

Plank, T., et al., *Proceedings of the Ocean Drilling Program, Initial Reports*, vol. 185, Ocean Drill. Program, College Station, Tex., 2000.

Révillon, S., S. R. Barr, T. S. Brewer, P. K. Harvey, and J. Tarney, An alternative approach using integrated gamma-ray and geochemical data to estimate the inputs to subduction zones from ODP Leg 185, Site 801, *Geochem. Geophys. Geosyst.*, *3*(12), 8902, doi:10.1029/2002GC000344, 2002.

Staudigel, H., S. R. Hart, H.-U. Schminke, and B. M. Smith, Cretaceous ocean crust at DSDP Sites 417 and 418: Carbon uptake from weathering versus loss by magmatic degassing, *Geochim. Cosmochim. Acta*, *53*, 3091–3094, 1989.

Staudigel, H., G. R. Davies, S. R. Hart, K. M. Marchant, and B. M. Smith, Large scale isotopic Sr, Nd and O isotopic anatomy of altered oceanic crust: DSDP/ODP sites 417/418, *Earth Planet. Sci. Lett.*, *130*, 169–185, 1995.

Staudigel, H., T. Plank, B. White, and H.-U. Schminke, Geochemical fluxes during seafloor alteration of the basaltic upper oceanic crust: DSDP Sites 417 and 418, in *Subduction: Top to Bottom*, *Geophys. Monogr. Ser.*, vol. 96, edited by G. E. Bebout et al., pp. 19–38, AGU, Washington, D. C., 1996.